

Fermilab

Fermi National Accelerator Laboratory
P.O. Box 500 • Batavia, Illinois • 60510

TD - 01 - 012
March 12, 2001

Mechanical Analysis of FF Arc-Quadrupole for VLHC Stage-2

Deepak Chichili

Abstract

The mechanical analysis of arc-quadrupole for VLHC stage-2 is discussed in this report. The magnet has a bore diameter of 43.5 mm with a nominal gradient of 400 T/m. The design is based on a $\cos(2\theta)$ coil structure made of Nb_3Sn superconductor with stand alone collared coil assembly. Iron yoke acts only as a flux return. The skin halves are welded on top of the iron yoke to form a helium vessel. Finite element analysis has been performed to optimize the coil prestress and to minimize the stress in major elements of coil support structure. The goal of this design is to develop a robust mechanical design, which will take in to account the manufacturing tolerances and uncertainties. Two different finite element schemes were considered, one with $1/8^{\text{th}}$ symmetry and the other with quarter symmetry of the coils. The idea was to cross check the analysis procedure with different boundary conditions.

1.0 Introduction

An FF arc quadrupole was designed for the VLHC stage 2 operations. The magnet bore diameter is 43.5 mm with a nominal gradient of 400 T/m at 27.2 kA. The design is based on a two-layer $\text{Cos}(2\theta)$ coil structure made of Rutherford-type Nb_3Sn cable and cold iron yoke. Fig. 1 shows the cable layout in the quadrupole. For more details on the magnet design refer to TD-01-019.

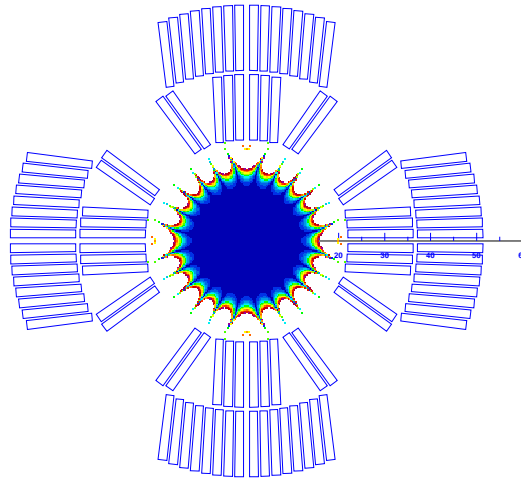


Fig. 1: Cable layout in the arc quadrupole.

Fig. 2 shows the schematic of the top quadrant of the magnet cross-section. The mechanical support structure consists of 20 mm thick collar laminations made of Nitronic-40 surrounded by iron yoke and stainless steel skin. The collar design is similar to that of LHC IR quadrupole (see Fig. 3). Large laminations and small laminations will be alternated, with small laminations filling the gaps in the pole region. This provides continuous support for the coils and also increases the longitudinal rigidity of the collar structure. The impregnated coil will be first enclosed by collar laminations, which are then locked in under pressure at two perpendicular directions by four pairs of tapered keys. This provides the necessary prestress to the coils. The two collared coil assemblies are then enclosed by two-piece iron yoke, which are radially supported by 5 mm thick stainless steel skin. Note that the outer diameter of the iron yoke is 530 mm. The yoke is aligned with the collared coils using alignment keys, which maintain some gap between the collars and the yoke laminations. Note that the collars give the entire prestress to the coils and the iron yoke acts only as a flux return. The skin halves are welded under some tension to provide good contact of the iron blocks. Skin alignment keys are installed between the skin shells for the longitudinal magnet alignment.

Finite element analysis using ANSYS was carried out to optimize the coil prestress and to minimize the stress in the collar laminations, which will then enable us to select the collar material. It is also important to estimate the magnet cross-section deformation during assembly at room temperature and during excitation at 4.2 K to understand its effect on magnet field quality.

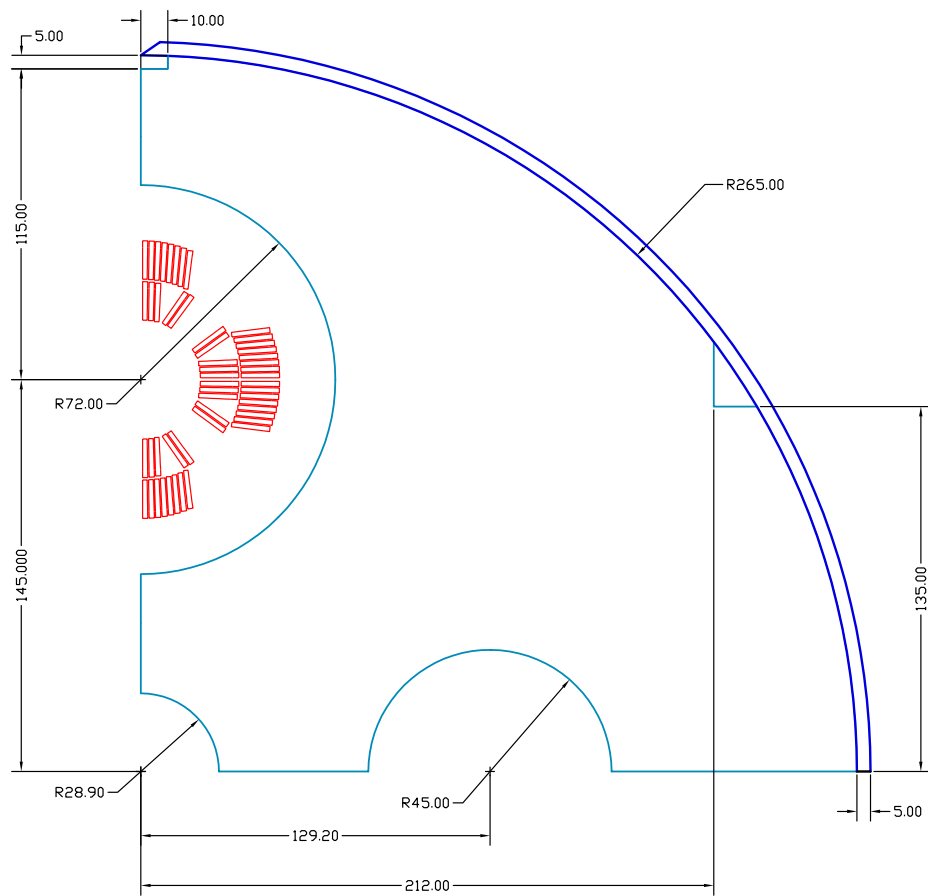


Fig. 2: Schematic of the top quadrant of the magnet.



Fig. 3: LHC IR quadrupole collar design.

2.0 Finite Element Model with 1/8th symmetry

Since the entire prestress to the coils is provided by the collar structure, each bore can be considered independently for modeling. Further due to symmetry it is sufficient to model 1/8 section of the bore. Fig. 4 shows the ANSYS model with 1/8th symmetry of the collared coil assembly.

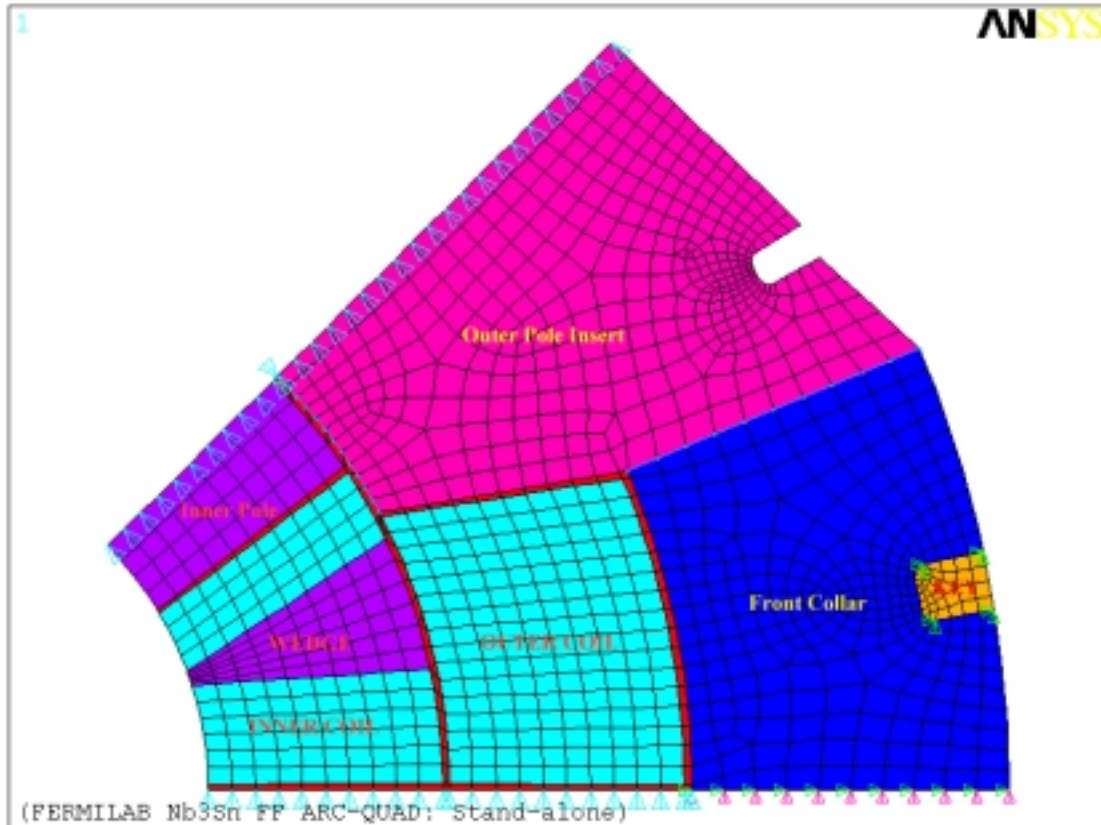


Fig. 4: ANSYS model of the collared coil quadrupole cross-section.

The following table lists the thermo-mechanical properties of different materials used in the model:

Material	E (300 K) GPa	E (4.2 K) GPa	Poisson's ratio	Thermal Contraction K ⁻¹
Coil	38	38	0.3	1.21 x 10 ⁻⁵
Ground Insulation	14	14	0.3	2.58 x 10 ⁻⁵
Inner Pole (Al Bronze)	108	113	0.3	1.21 x 10 ⁻⁵
Wedges (Al Bronze)	108	113	0.3	1.21 x 10 ⁻⁵
Collar (Nitronic-40)	190	210	0.3	0.90 x 10 ⁻⁵

Table 1: *Thermo-Mechanical properties of the materials used in the model.*

2.1 Model Description

The model includes inner and outer layer of coils, interlayer and ground insulation, two layers of collar laminations, pole insert and one key. The inner and outer layers of coils along with the inner pole piece are glued to form a coil structure. The mechanical support structure for the coils consists of three parts. In the top layer we have a pole insert (smaller lamination) and a section of the larger collar lamination. In the bottom layer we have only the larger collar lamination (which has the in-built pole insert). Two simulate the multi-layer structure of collar laminations in 2D; a 1 mm thick layer was meshed for the coil structure and the key whereas simulating two layers of a 0.5 mm thick mesh created the collar structure. Note that the plane-stress with thickness option was used. The areas were meshed with two-dimensional elements (Plane 42) and the contact surfaces with CONTACT 48 elements. Having radial interference between the collar structure and the outer layer of coil and azimuthal interference between the pole and the outer layer provided the prestress to the coils. The radial interference was obtained through one-dimensional contact elements, COMBIN 40 oriented perpendicular to the interface. The azimuthal interference between the pole and the outer layer was obtained through CONTACT 52 elements. Note that while COMBIN 40 elements are frictionless contact elements, CONTACT 52 are frictional contact elements. A friction coefficient of 0.1 was used in the analysis.

The appropriate boundary conditions were chosen to reflect the mechanical design. Symmetry boundary conditions were applied along the entire 45° line and for coils at the mid-plane. The two layers of collars were coupled to the key both in radial and azimuthal direction using CP command. Both CP and CE commands were used for the collars at the mid-plane to satisfy rotational symmetry. Note that the two layers of collars at the mid-plane have same radial displacement and hence CP was used to couple nodal displacements along radial direction. However they have same azimuthal displacements but in opposite directions ($u_{\theta 1} + u_{\theta 2} = 0$) and hence CE command was used to impose this boundary condition.

The first step was to evaluate the Lorentz force distribution in the coils at 27.2 kA, which corresponds to a gradient of 400 T/m. Note that the same mesh for the coil will be used for magnetic and mechanical analysis so that the nodal forces can be easily applied.

2.2 Lorentz Forces

A quadratic mesh was used in all coil blocks and wedges. Inside each block of coil, the number of elements in azimuthal direction is equal to twice the number of turns. Each coil block is assumed to have a uniform current distribution and the corresponding current density was computed from the current in each cable times the number of turns in that block. The direction of the current density was applied to reflect the FF configuration of the arc quadrupole. Permeability of iron as a function of magnetic field was used in this analysis. Fig. 5 shows the Lorentz force distribution in the $1/8^{\text{th}}$ section of the coil at a gradient of 400 T/m (which corresponds to 27.2 kA of cable current). Table 2 shows the forces in the three blocks computed with ANSYS and with of OPERA. The slight

difference in the values is because the holes in the iron yoke were not added in the ANSYS model. Fig. 6 shows the flux lines in the magnet cross-section. Note that the direction of the flux lines satisfies the FF configuration of the 2-in-1 arc quadrupole.

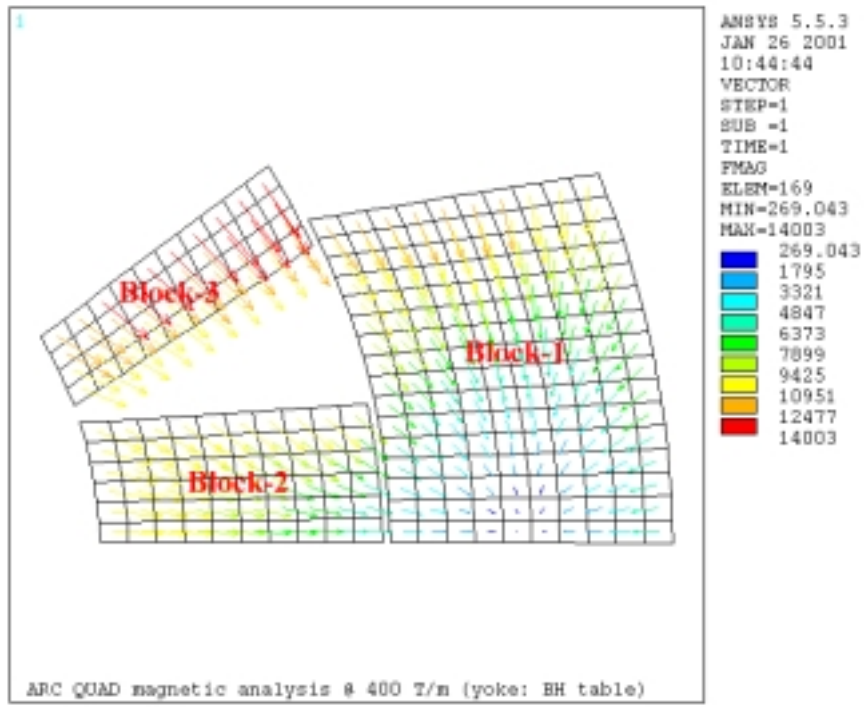


Fig. 5: Lorentz force distribution in the coil cross-section.

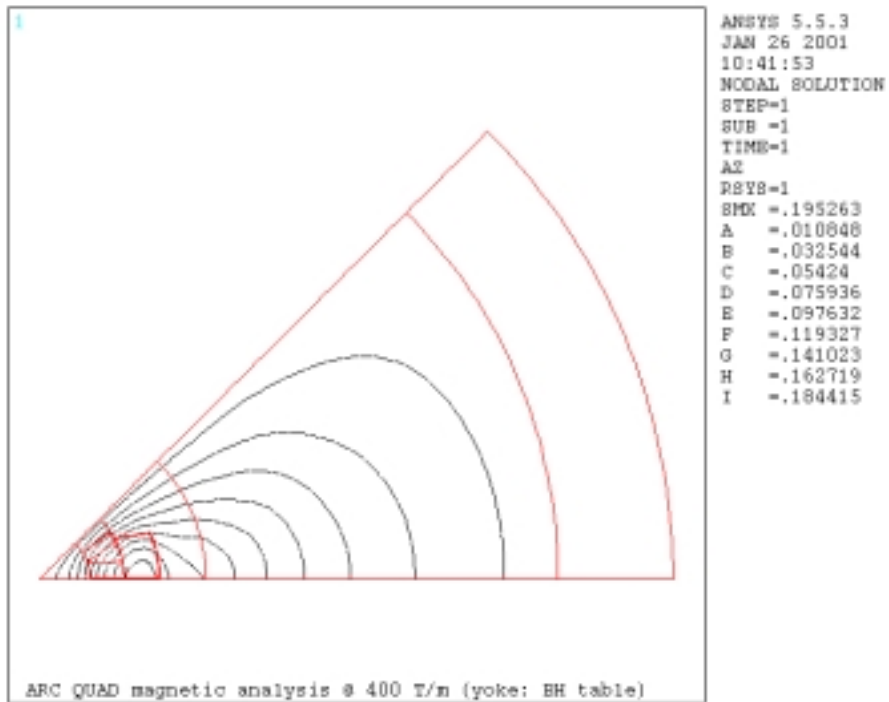


Fig. 6: Flux distribution in the magnet cross-section.

Cable Block Number	ANSYS, kN/m		OPERA, kN/m	
	F _x	F _y	F _x	F _y
Block-1	171.137	-829.627	170.175	-832.77
Block-2	487.139	-172.914	485.966	-175.05
Block-3	344.940	-304.129	345.488	-304.86
Total	1003.21	-1306.67		

Table 2: Lorentz Forces in 1/8th section of the coil.

2.3 Mechanical Analysis

The interference between the coil and collar determines the amount of prestress in the coils. Typically this is achieved during production through oversize in coil outer diameter. This means an oversized coil is compressed while the keys are inserted into collars. The reaction from the coils forces the collars to expand beyond the nominal loose collar dimensions. The amount of collar deflection is directly proportional to the coil prestress. Hence during magnet production the collar deflection measurements are a good measure to estimate the coil prestress. The goal of this analysis was to find an optimum interference between the coil and the collar laminations.

The acceptable solution should meet the following criteria:

1. The peak stress in the coil should not exceed 150 MPa at all stages of the magnet operation.
2. A minimum coil stress of 5 to 10 MPa at full gradient to ensure that coils do not unload.
3. The maximum collar stress should not exceed the yield stress of the collar material.

After several iterations, the optimum interference between the coil and the collar was found to be 0.15 mm in the radial direction and 0.025 mm in the azimuthal direction. Fig. 7 shows the azimuthal stress distribution in the coil at room temperature after assembly, at 4.2 K and 0 T/m and at 4.2 K and nominal gradient, 400 T/m. Table 3 lists the average azimuthal stress values in the coil during various stages of the magnet.

Stages	Mean Azimuthal Stress, MPa			
	Inner layer		Outer Layer	
	Pole	Mid-Plane	Pole	Mid-Plane
293 K	112	69	50	73
4.2 K, 0 T/m	93	66	39	57
4.2 K, 400 T/m	45	78	14	78

Table 3: Average azimuthal stress in the coil.

Fig. 8 shows the radial displacement of the coil assembly at various stages of the magnet. Note that the difference in radii between the mid-plane and the pole for the inner bore is only 11 μm at 4.2 K, 0 T/m. At 4.2 K, 400 T/m, the inner bore returns to its circular shape. Table 4 lists the radial displacement of the coil at four different positions (the positions are shown in Fig. 8).

Stages	Radial Displacement, μm			
	Inner layer		Outer Layer	
	1	2	3	4
293 K	-55	-41	-69	-69
4.2 K, 0 T/m	-125	-114	-219	-219
4.2 K, 400 T/m	-103	-103	-214	-214

Table 4: Radial displacements of the coil at four positions.

The Von-Mises stress distribution in the collar after assembly at room temperature is shown in Fig. 9. The peak stress in the collar is about 600 MPa except at the locations where the nodes were coupled to the key. The radial displacements of the collar at various stages of the magnet are shown in Fig. 10 and Table 5 lists the average radial displacements of the collar at mid-plane and pole region. For an average inner layer pole stress of 112 MPa and an outer layer pole stress of 50 MPa (both at room temperature after collaring), the collar deflects by about 76 μm in the mid-plane. This is equivalent to 1.47 MPa/ μm for inner layer pole and 0.66 MPa/ μm for outer layer pole.

Stages	Collar Radial Displacement, μm	
	Pole	Mid-Plane
293 K	78	76
4.2 K, 0 T/m	-123	-134
4.2 K, 400 T/m	-119	-125

Table 5: Radial displacements of collar.

Lastly, the stress in the coil during collaring operation needs to be estimated to understand the relaxation of the coil assembly after collaring. This was simulated by applying zero displacement boundary condition to the outer surface of the collar in addition to the already existing ones. The average inner layer and outer layer pole stress during collaring was about 202 MPa and 150 MPa respectively. Note that the average stress after collaring was 112 MPa in the inner layer pole region and 50 MPa in the outer layer pole region. This indicates that we retain only 55% in the inner layer pole region and 33% in the outer layer pole region. Note that the analysis to compute stress in the coils during collaring assumes a square key. However in production we could achieve same prestress in the coils after collaring using tapered keys without having to over-compress during collaring. This could eliminate the need to compress the coils over 150 MPa. This procedure needs to be verified on a mechanical model.

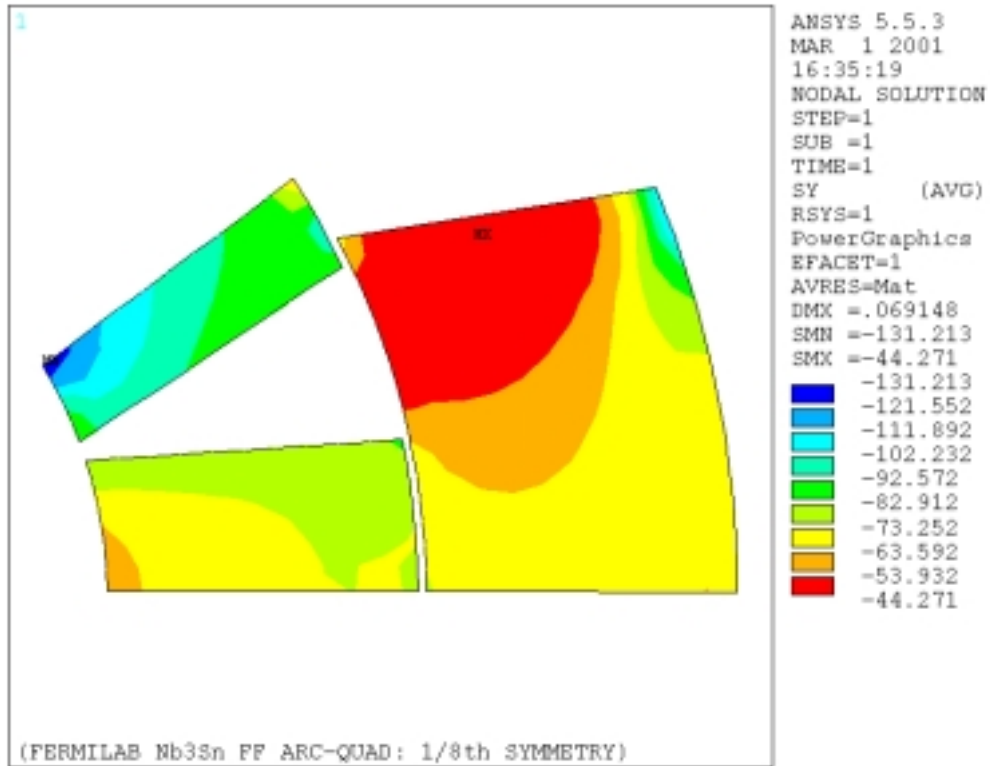


Fig. 7 (a): Azimuthal stress distribution in the coil at 293 K (after collaring)

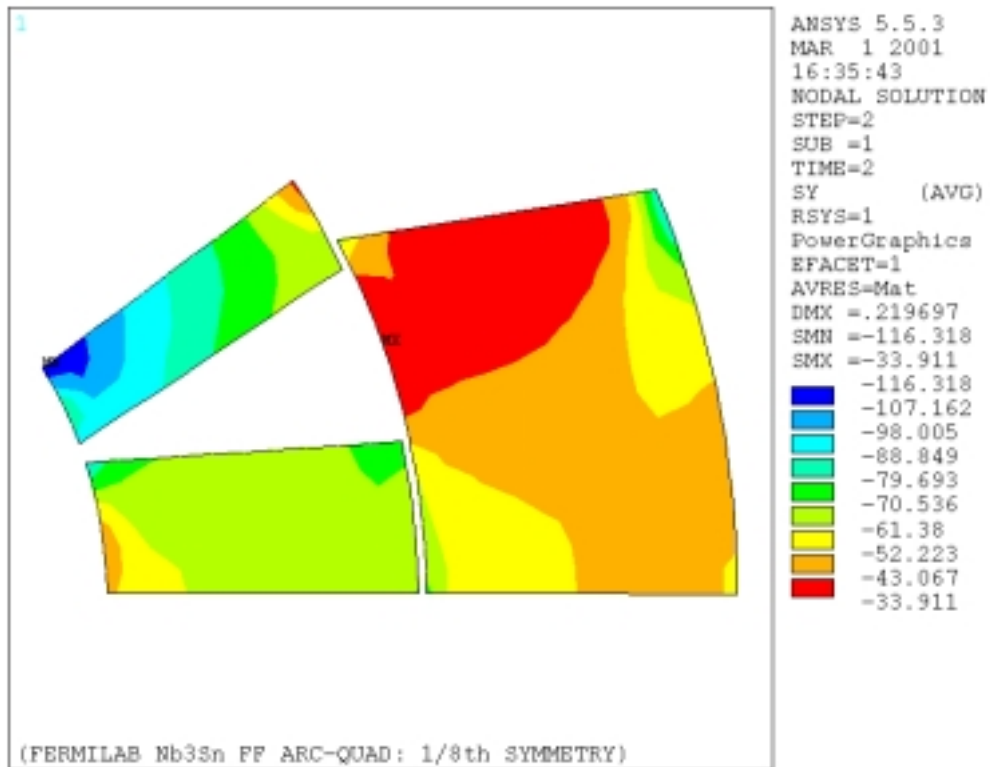


Fig. 7(b): Azimuthal stress distribution in the coil at 4.2 K, 0 T/m

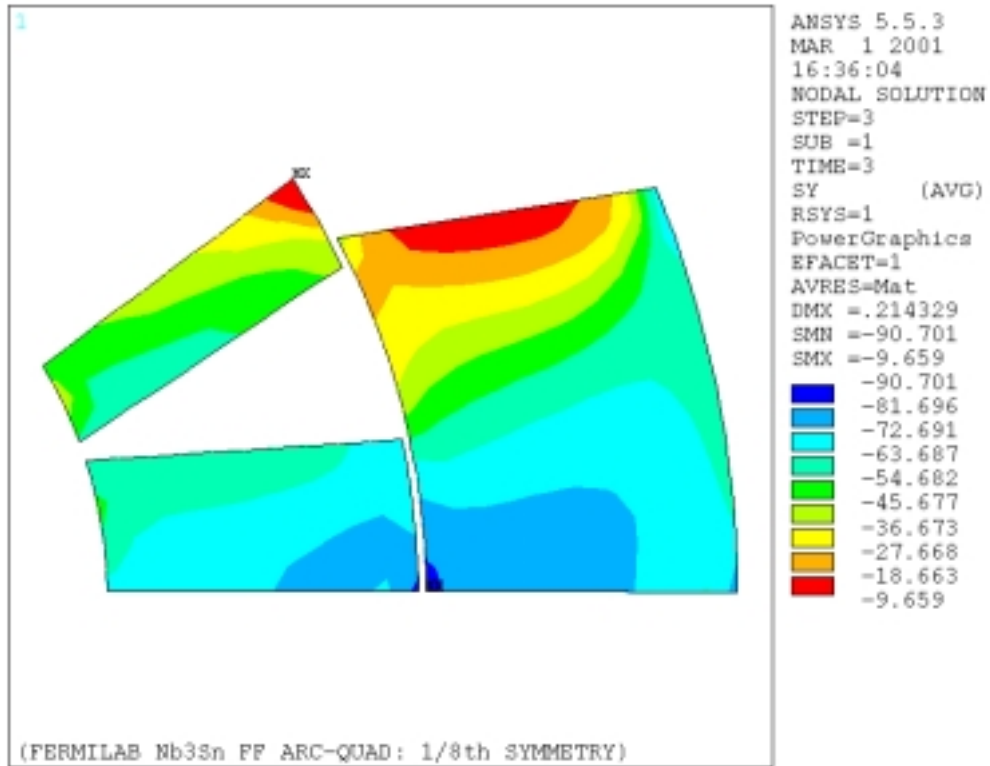


Fig. 7(c): Azimuthal stress distribution in the coil at 4.2 K, 400 T/m

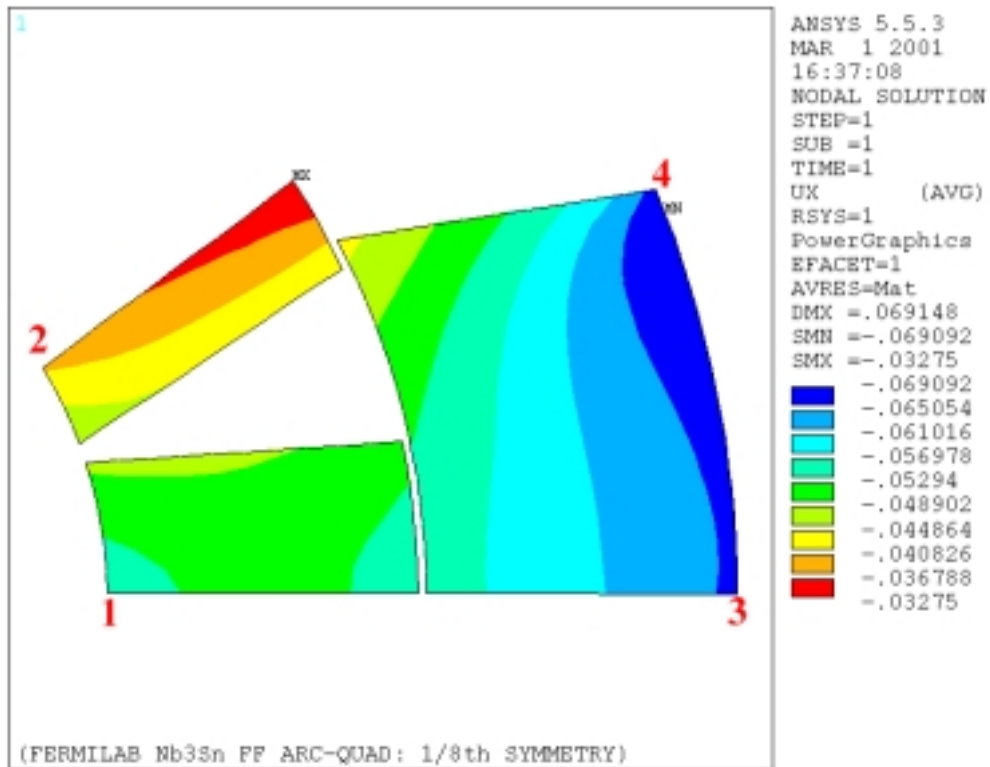


Fig. 8(a): Radial displacement of the coil at 293 K (after collaring).

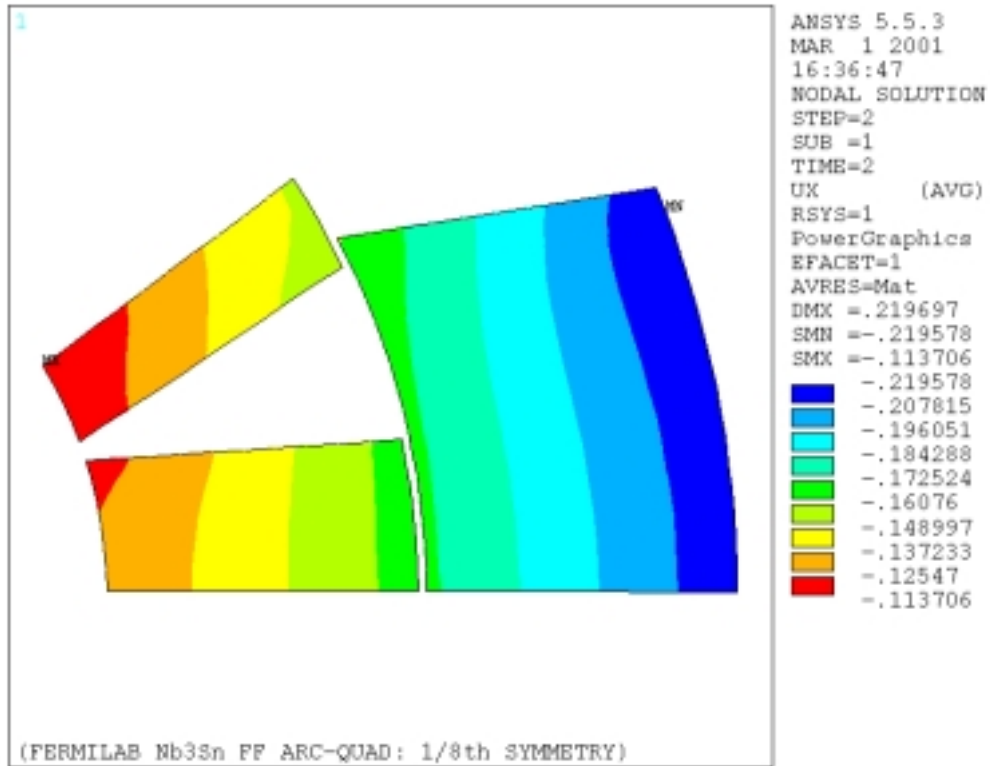


Fig. 8(b): Radial displacement of the coil at 4.2 K, 0 T/m.

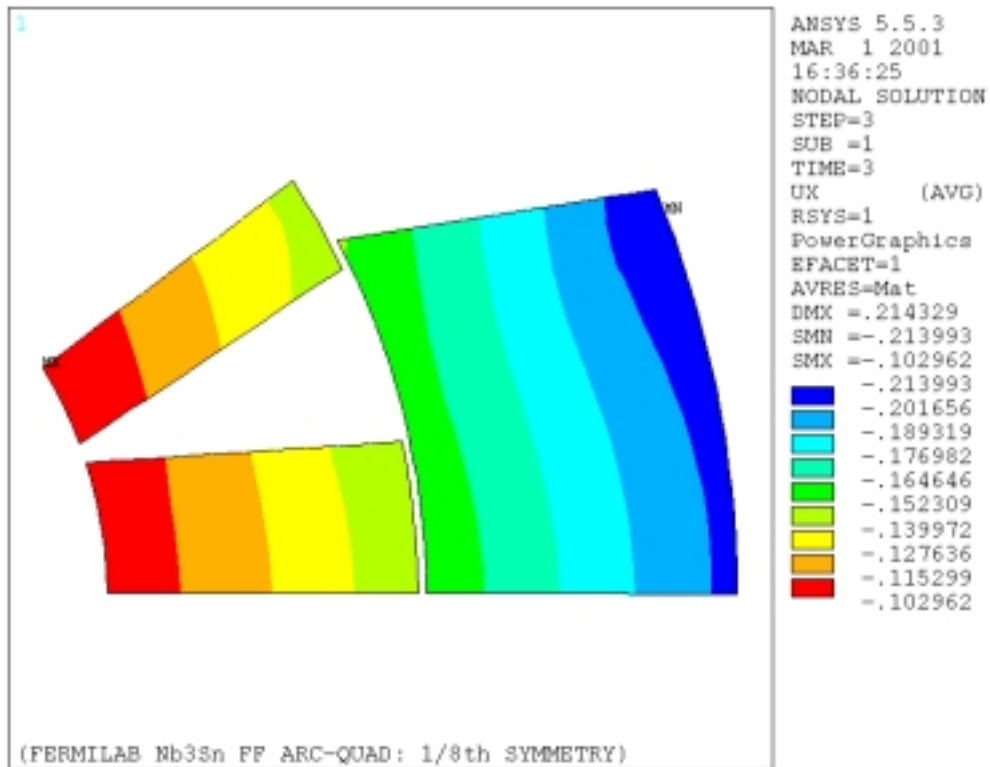


Fig. 8(c): Radial displacement of the coil at 4.2 K, 400 T/m.

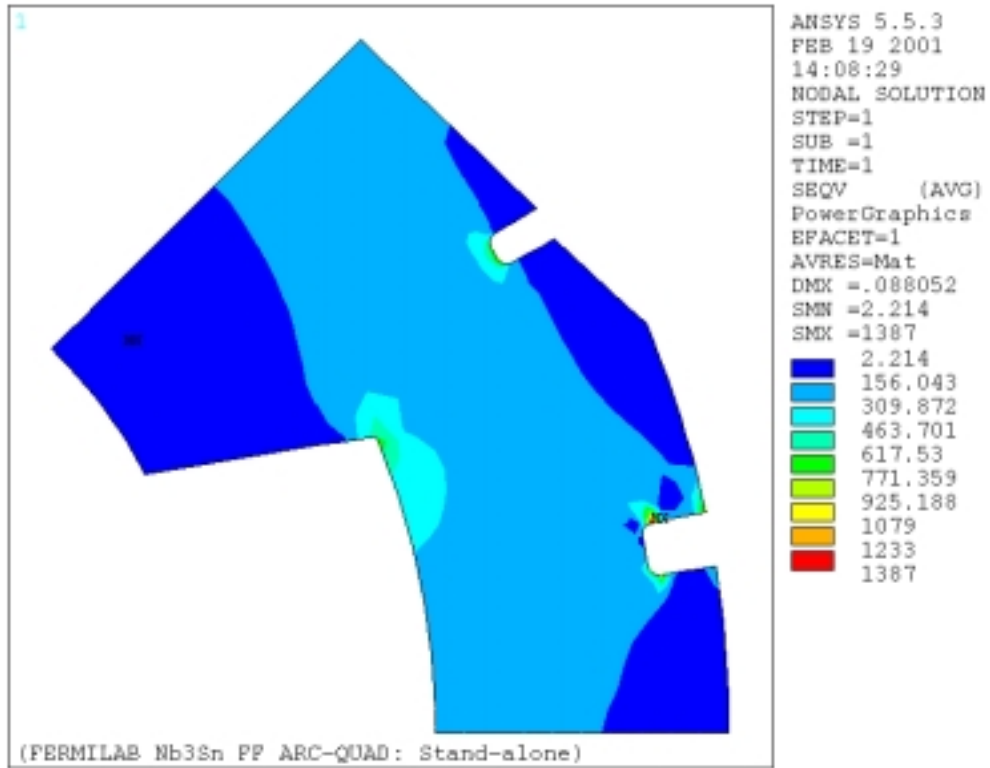


Fig. 9: Von-Mises stress distribution in the collar after collaring at room temperature.

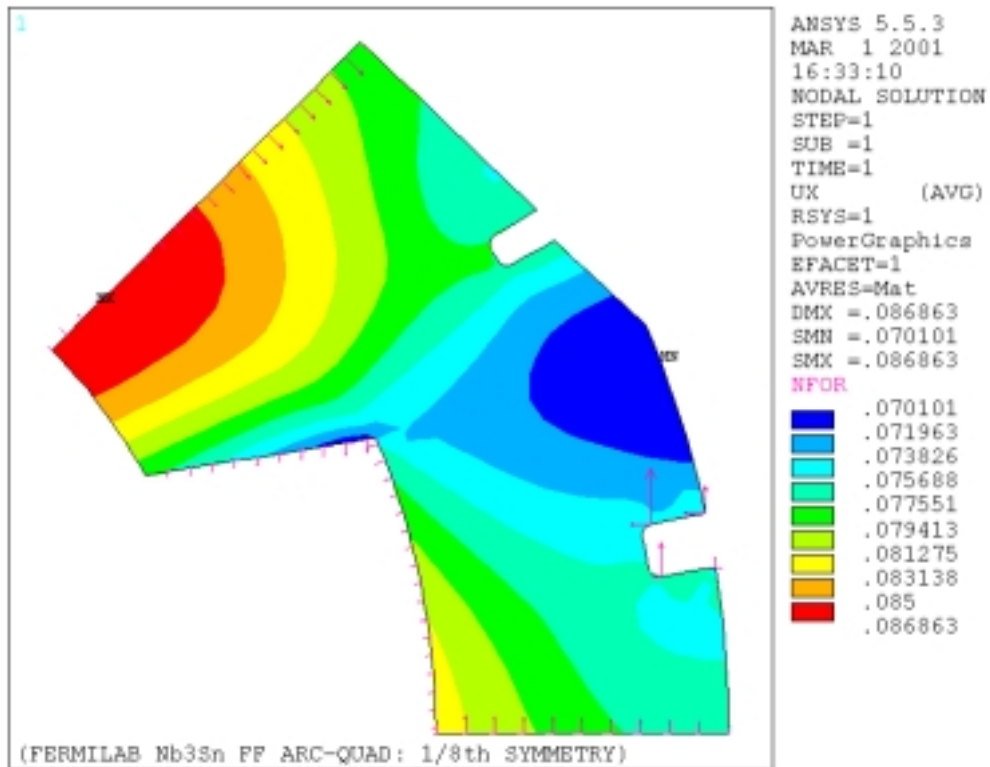


Fig. 10(a): Radial displacement of the collar at room temperature after collaring.

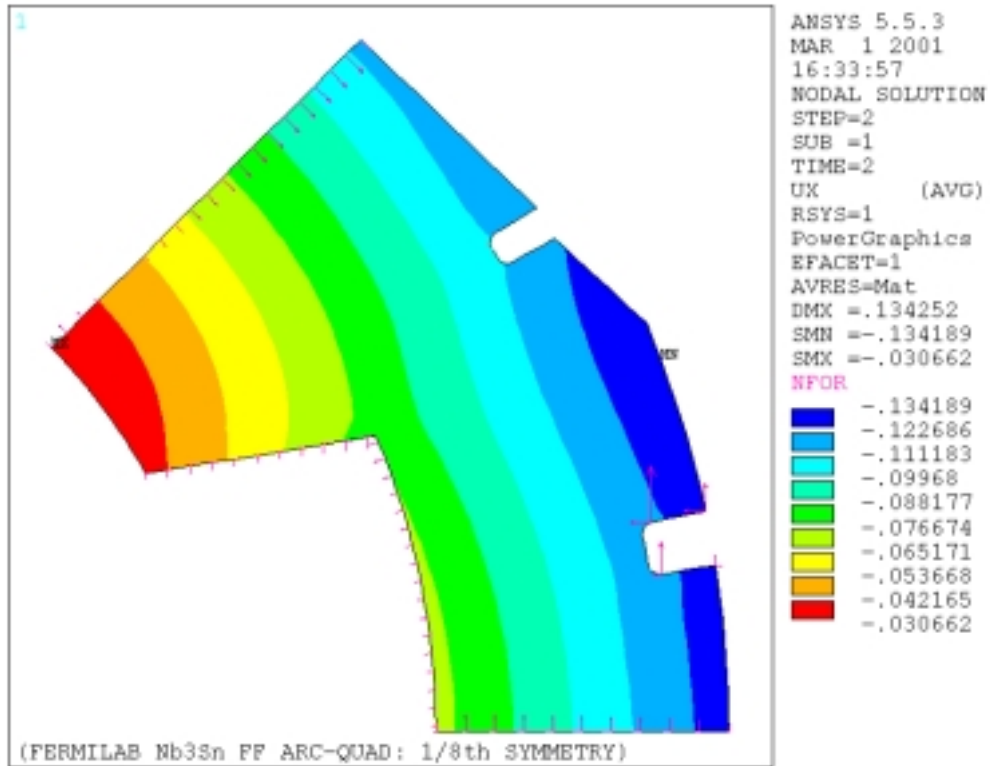


Fig. 10(b): Radial displacement of the collar at 4.2 K, 0 T/m.

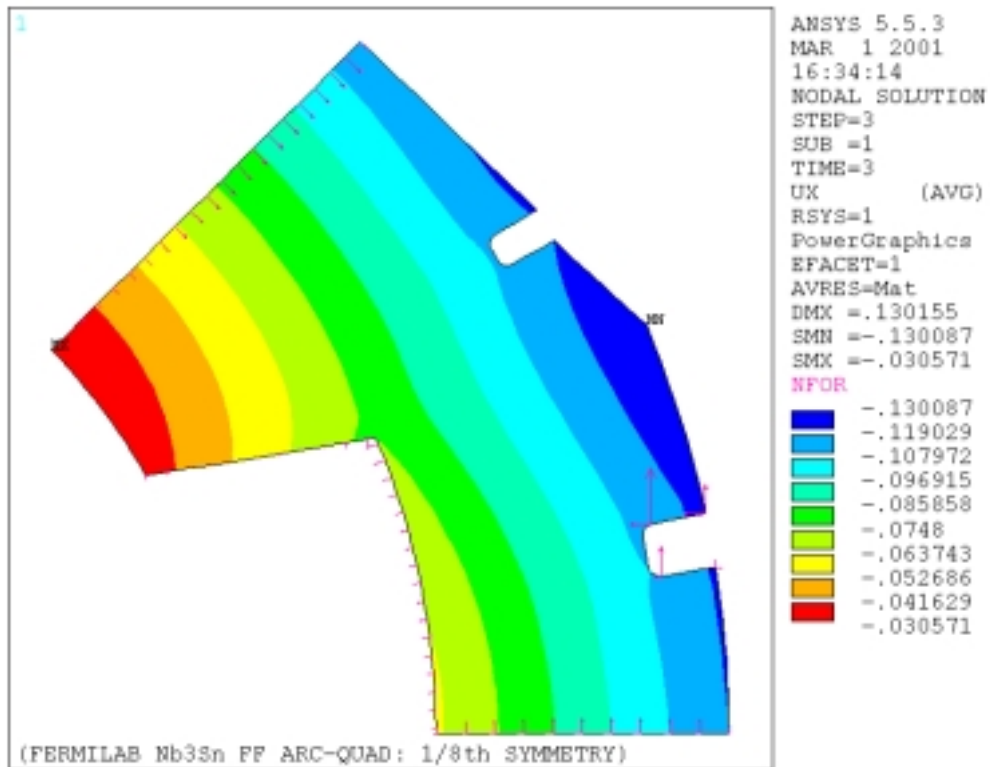


Fig. 10(c): Radial displacement of the collar at 4.2 K, 400 T/m.

3.0 Finite Element Model with Quarter symmetry

The second version of the analysis was done with the quarter symmetry of the coils (in a single bore). The two different models were constructed to check the validity of the boundary conditions applied during the analysis. Fig. 11 shows the ANSYS model.

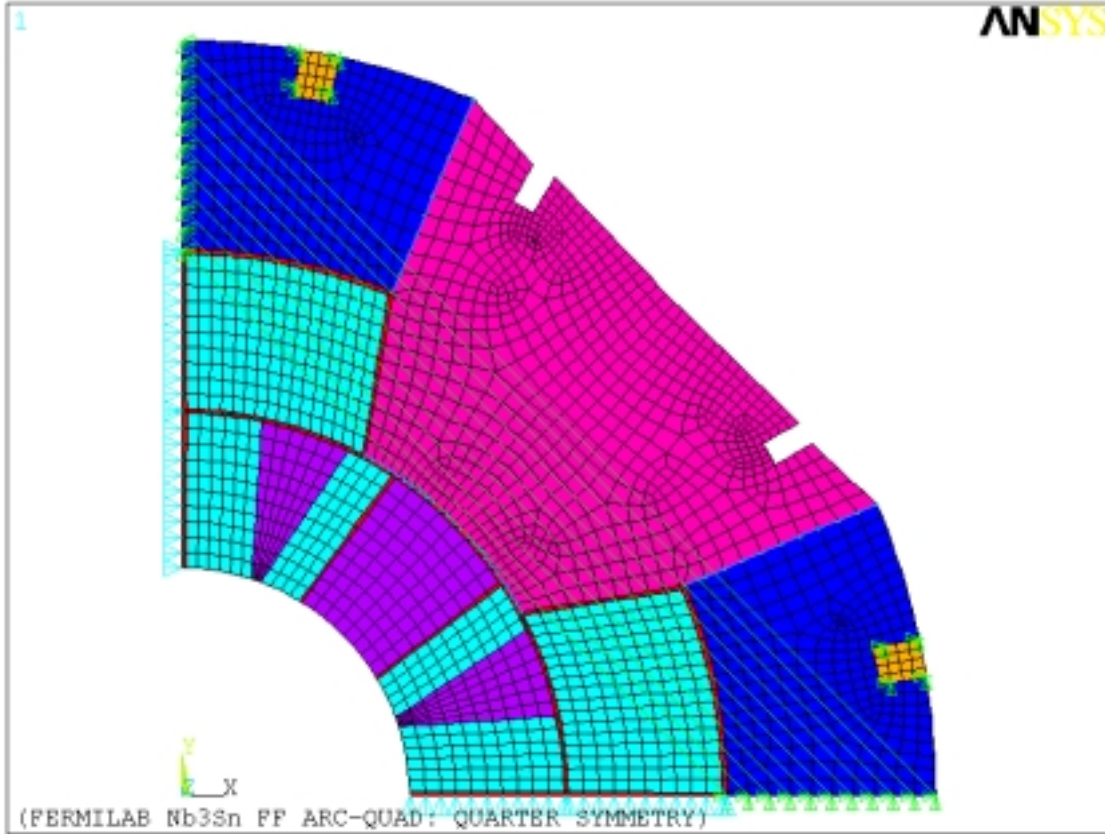


Fig. 11: ANSYS model for quarter symmetry of the coils.

The following are the boundary conditions used for this model; symmetry boundary conditions were used for the coils at 0° and 90° . The radial and azimuthal displacements of the front collar at 0° are coupled to that of the back collar at 90° . Similarly the radial and azimuthal displacements of the back collar at 0° are coupled to that of the front collar at 90° . Finally the front and back collars are coupled to the keys both in the radial and azimuthal directions.

A radial interference of 0.15 mm and an azimuthal interference of 0.025 mm were applied similar to that in the previous ANSYS scheme. Note that if the boundary conditions were chosen correctly, the two ANSYS schemes should give identical results. This would be a check on the models. Fig. 12 shows the azimuthal stress distribution in the coil cross-section and Fig. 13 shows the radial displacement of the collar lamination at various stages of the magnet operation. The two schemes give similar results, which indicates that the boundary conditions chosen during the analyses are correct.

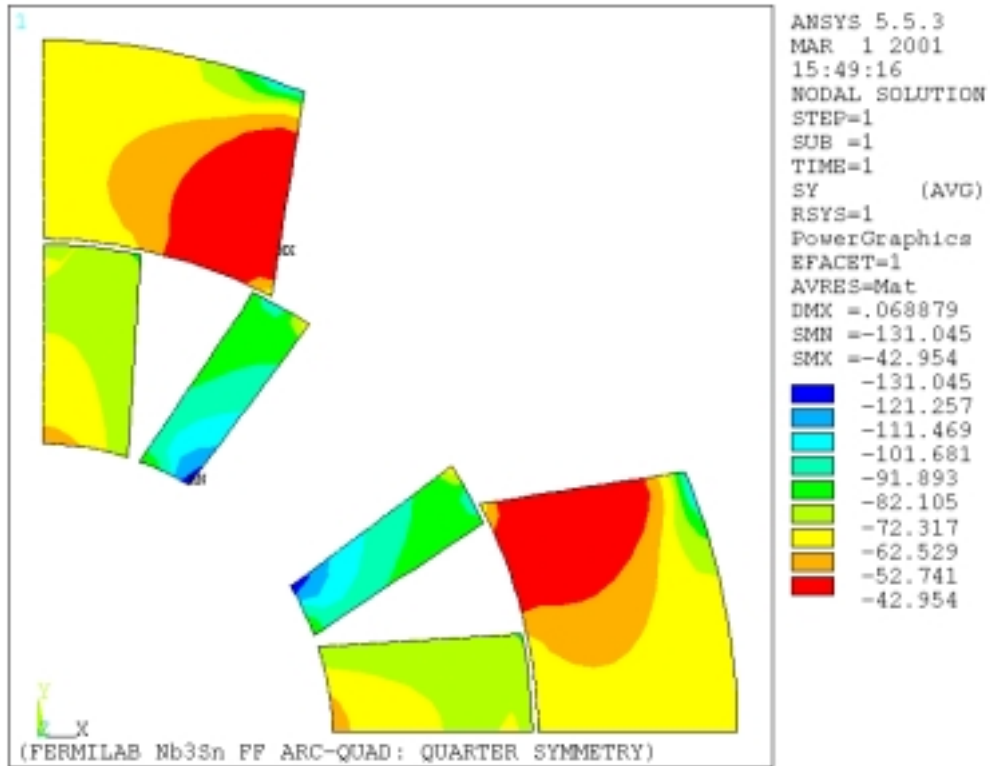


Fig. 12 (a): Azimuthal stress distribution in the coil at 293 K (after collaring)

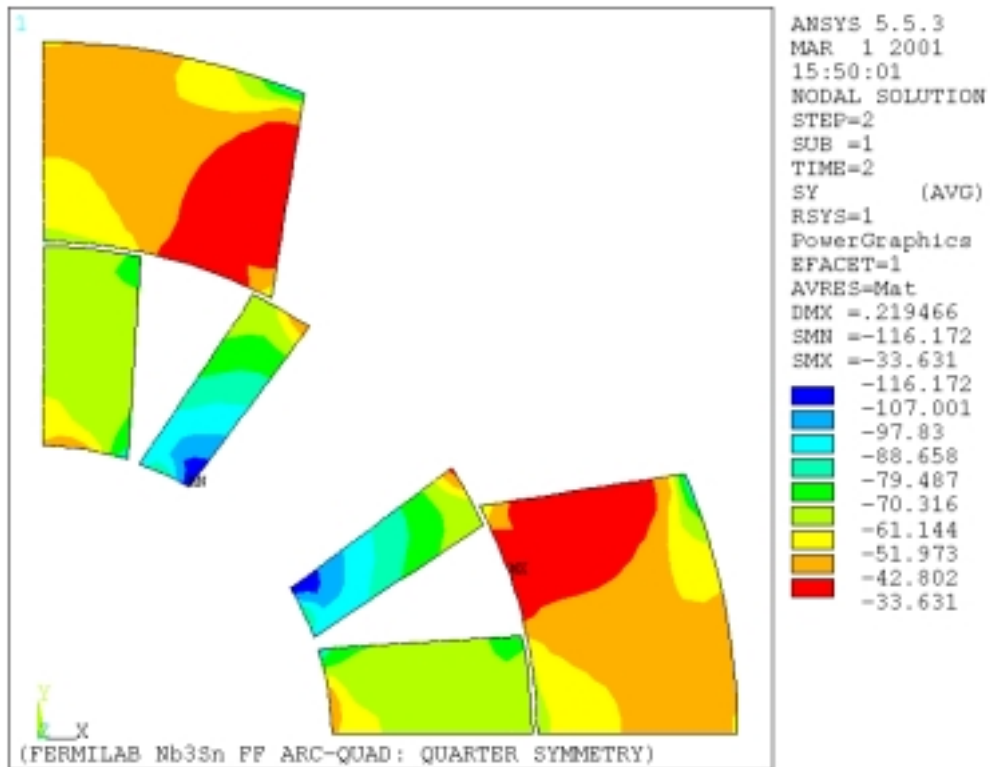


Fig. 12(b): Azimuthal stress distribution in the coil at 4.2 K, 0 T/m

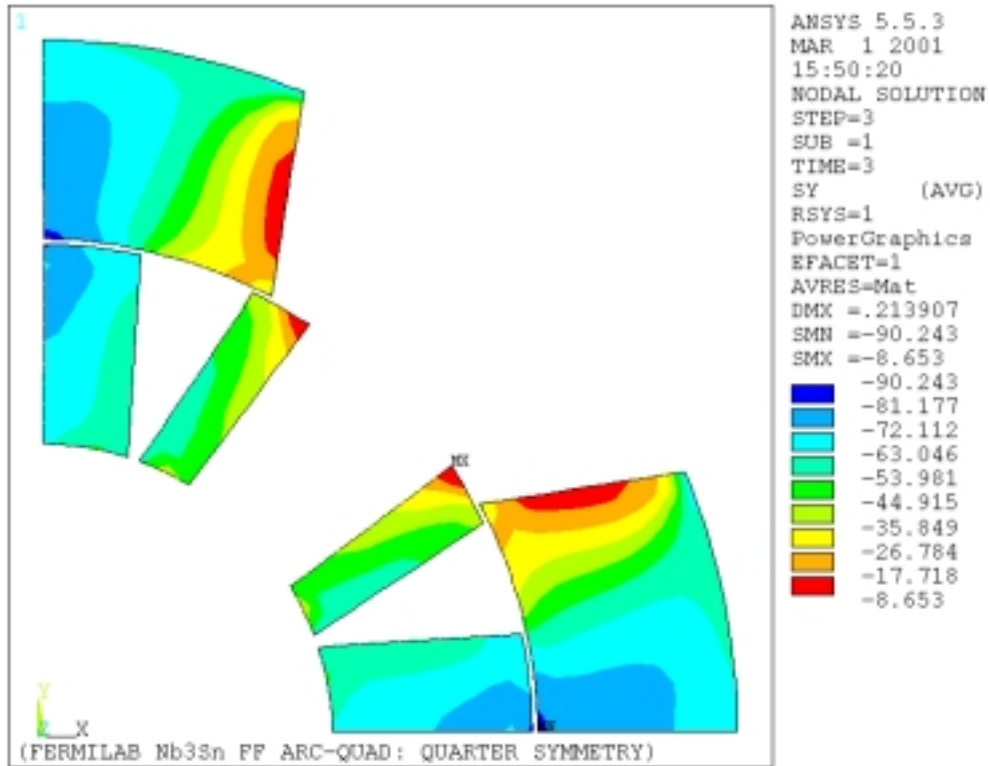


Fig. 12 (c): Azimuthal stress distribution in the coil at 4.2 K, 400 T/m

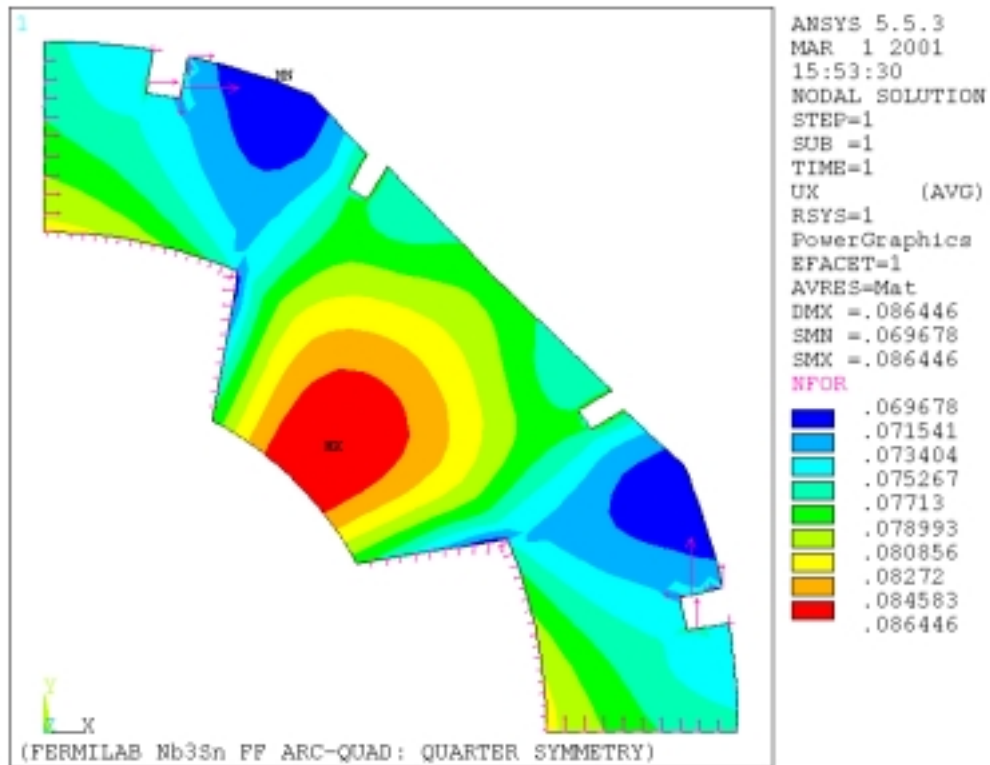


Fig. 13(a): Radial displacement of the collar lamination after assembly.

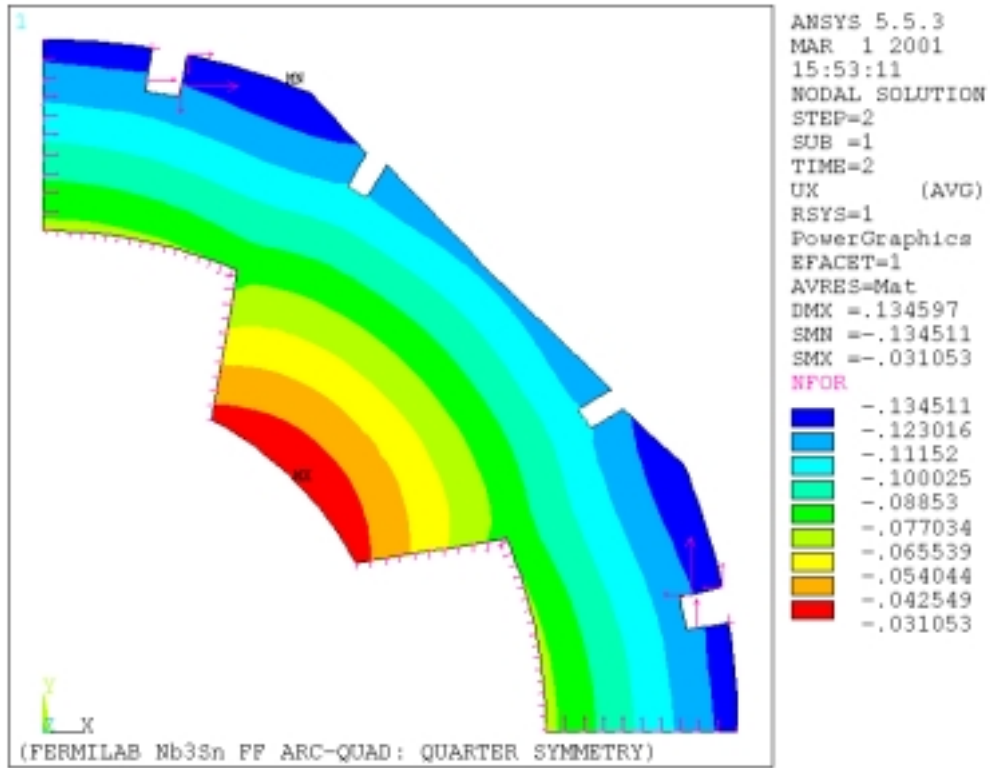


Fig. 13(b): Radial displacement of the collar lamination at 4.2 K, 0 T/m.

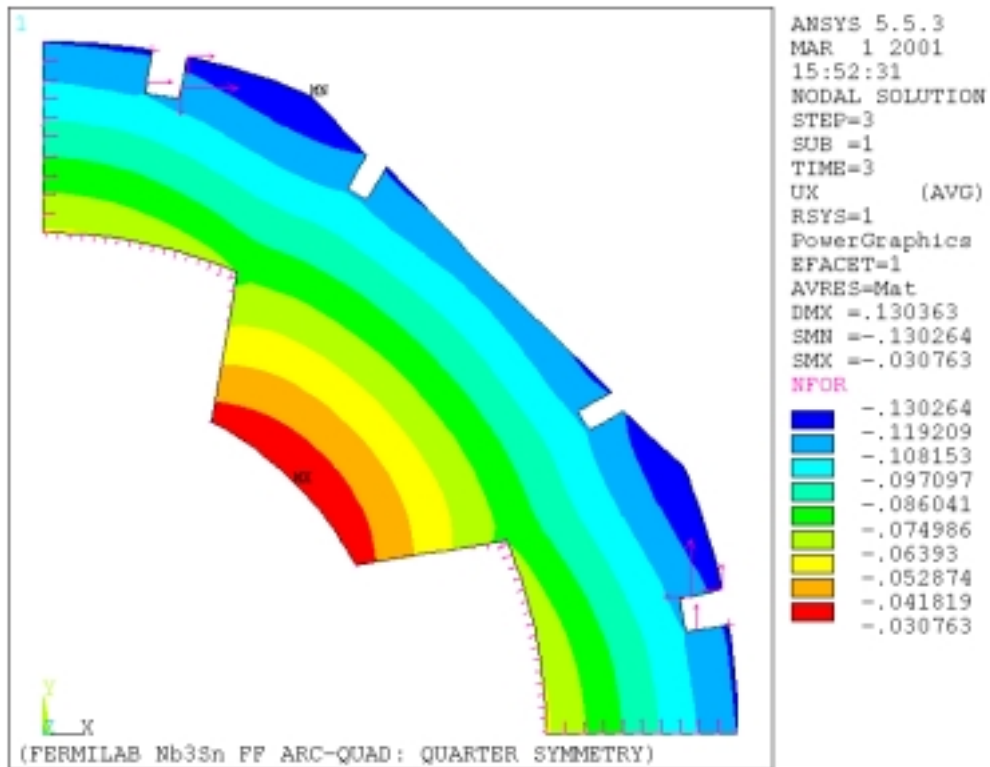


Fig. 13(c): Radial displacement of the collar lamination at 4.2 K, 400 T/m.

4.0 Summary

A detailed finite element analysis has been performed to optimize the stresses in the coil and in the collar laminations. A design similar to the LHC IR quadrupole works for the Nb₃Sn arc quadrupole. The thickness of the collar laminations is about 20 mm. The choice of material would be Nitronic-40 due to high stresses near the keys.

A second version of the design is underway in which the coils in a given cross-section will be supported by two large collar laminations with two pole inserts. This design, similar to the LHC arc-quadrupole design, will ease the collar stacking process.